

Article

Trace Element Evidence of Subduction-Modified Mantle Material in South Mid-Atlantic Ridge 18–21°S Upper Mantle

Tianxiao Ji ^{1,2} and Zhigang Zeng ^{1,2,3,*}

- ¹ Seafloor Hydrothermal Activity Laboratory, CAS Key Laboratory of Marine Geology and Environment, Institute of Oceanology, Chinese Academy of Sciences, Qingdao 266071, China
² University of Chinese Academy of Sciences, Beijing 100049, China
³ Laboratory for Marine Mineral Resources, Qingdao National Laboratory for Marine Science and Technology, Qingdao 266071, China
* Correspondence: zgzeng@ms.qdio.ac.cn

Abstract: Mid-ocean ridge basalts (MORBs), produced at mid-ocean ridge where the continents and subduction zones are distant, are the product of partial melting of the upper mantle and their chemical composition can provide information about the mantle itself. The geochemical characteristics of MORBs enable us to be more informed about the geological processes of the upper mantle below the mid-ocean ridge, and assist us in understanding mantle heterogeneity and geodynamic processes. In this paper, new data of major elements, trace elements, and Nd-Hf isotopes of south mid-Atlantic ridge (SMAR) 18–21°S MORBs are presented. TAS diagram shows that the samples belong to subalkaline basalt compositional field. Trace elements (e.g., $(La/Sm)_N = 0.49–0.79$) show that the samples are N-MORBs. However, the primitive mantle-normalized trace element patterns showed that the studied samples were clearly enriched in Rb, U, Pb, and other fluid-mobile elements. Meanwhile, the trace element ratios, such as Nb/U and Ce/Pb, are also significantly different from the typical N-MORB. Combined with the Nd-Hf isotopic composition, we propose that these anomalies are not related to continental crust material, delaminated subcontinental lithospheric mantle (SCLM), recycled sediments, direct supply of mantle plume, nor are they the result of subduction directly affecting the mantle source, but are caused by the incorporation of mantle material modified by subduction.



Citation: Ji, T.; Zeng, Z. Trace Element Evidence of Subduction-Modified Mantle Material in South Mid-Atlantic Ridge 18–21°S Upper Mantle. *J. Mar. Sci. Eng.* **2023**, *11*, 441. <https://doi.org/10.3390/jmse11020441>

Academic Editor: Sergio Bonomo

Received: 30 December 2022

Revised: 17 January 2023

Accepted: 17 January 2023

Published: 17 February 2023



Copyright: © 2023 by the authors. Licensee MDPI, Basel, Switzerland. This article is an open access article distributed under the terms and conditions of the Creative Commons Attribution (CC BY) license (<https://creativecommons.org/licenses/by/4.0/>).

Keywords: south mid-Atlantic ridge (SMAR); mid-ocean ridge basalt (MORB); subduction; mantle heterogeneity

1. Introduction

Mantle is heterogeneous. Isotopically, the mantle can be divided into depleted MORB mantle (DMM), enriched mantle 1 and 2 (EM1 and EM2), high $\mu' = {}^{238}\text{U}/{}^{204}\text{Pb}$ (HIMU), and other mantle end-members [1,2]. Different plumes have different characteristics of enriched mantle end-members. For example, St. Helena plume is the representative of HIMU mantle end-members, and Tristan-Gough plume represents the EM1 mantle end-members [3,4]. OIB is the product of the mantle plume, and its geochemical composition can indicate the origin of the mantle end-member. For example, HIMU mantle end-members are usually hypothesized to be associated with the recycled oceanic crust [3]. MORBs are derived from the DMM, and are produced at the mid-ocean ridge [5] which is distant from continents and subduction zones. Therefore, the composition of MORBs is less contaminated by the continental material and subduction associated process, and is generally considered to be relatively uniform. However, increasing evidence [6–12] is showing that the mantle source of MORB is not as uniform as initially hypothesized and it is even heterogeneous at different scales. Dupre and Allegre [6] found that the Pb and Sr isotopic compositions of MORBs from the Indian Ocean are more radioactive than MORBs from the other ocean. Mougél et al. [12] sampled the East Pacific Rise (EPR) segment at a high density within the

length of only 15 km, and found that the MORB source region was highly heterogeneous even at this small scale. Subduction of oceanic plate, detachment of SCLM, and mantle plume are the reasons of upper mantle heterogeneity [4,12–22]. Studying which process could cause upper mantle heterogeneity can assist us in understanding the dynamics of the Earth.

The more incompatible the elements are, the more inclined they are to enter the melt phase during melting and crystallization. Elements with similar compatibility (such as Ce and Pb, Nb and U, etc.) have little relative change in their contents in rocks due to their similar geochemical behavior in magmatic processes. Therefore, the ratio of these element pairs in rocks is basically unchanged compared with their mantle source, and can be used to reflect the chemical composition characteristics of the source area [13]. Nb/U and Ce/Pb ratios of MORBs are relatively uniform [13,23,24], and significantly higher than those of the continental material and island arc volcanics [13]. Therefore, the anomalies in the ratios of Nb/U and Ce/Pb in MORB can be used as indicators of contamination caused by recycled sediments, delaminated subcontinental lithospheric mantle, continental crust material, and subduction of oceanic plate.

Yang et al. [21] proposed a back-arc basin basalt (BABB) filter based on Nb/U, Ce/Pb, Rb/Nb, and Ba/Nb ratios. Using this filter, it was found that BABB-like MORBs are widespread in the Atlantic, Indian, and Arctic oceans, but rare in the Pacific. This compositional distribution is explained by the subduction shield model around the Pacific Ocean. Circum-Pacific subducted slabs are mostly continuous for at least the last 180 million years and at least to transition zone depth, and would strictly limit the contribution of the slab flux to sub-Pacific mantle [21]. In this model, the mid-Atlantic (from ~33°N to ~34°S) is hardly affected by subduction due to the presence of a slab window (the subduction of the Chile ridge). However, the slab window does not exist since the Pacific subduction began. Was the mid-Atlantic mantle really not affected by subduction?

In this study, we present new whole-rock major element, trace element, and Nd-Hf isotope data of SMAR 18–21°S MORBs, combined with published geochemical data, to investigate whether the area was affected by subduction.

2. Geological Background and Samples

The South Atlantic is located between Africa and South America (Figure 1), with Olavtoppen Island at the southernmost end and Romanche Trench at the northernmost end, which gradually opened from south to north during the breakup of west Gondwana from ~134 Ma [25,26]. There are several hotspots in the South Atlantic including Ascension, Circe, St. Helena, Tristan, Discovery, and Shona (yellow circles in Figure 1), among which St. Helena is closest to the study area. The St. Helena hotspot is linked by the St. Helena seamount chain to West Africa, but there is no corresponding continent flood basalt [27] (Figure 1). Geochemically, St. Helena is a mantle plume with typical HIMU mantle end-member characteristics. Mantle plumes in the South Atlantic have extensive effects on different ridge segments of SMAR [28–30], and are associated with the breakup of Gondwana [31].

During the China Ocean Survey (COS) Expeditions No. 22 and 26 cruises of the R/V DAYANGYIHAO, 16 MORBs from 14 stations in this study were collected by TV-grab (TVG) at depths of 2075–3386 m from the axis of the SMAR 18–21°S, which is located at the extension line of St. Helena seamount chain and 750 km from St. Helena Island. The main rock types of this area include N-MORB and E-MORB, but the radioisotope compositions, especially the $^{206}\text{Pb}/^{204}\text{Pb}$ ratio, are more radioactive than those of typical MORBs, indicating that these basalts are clearly affected by enriched components [26,32,33]. At present, the St. Helena plume is still affecting the upper mantle beneath the study area through fluid channels [26].

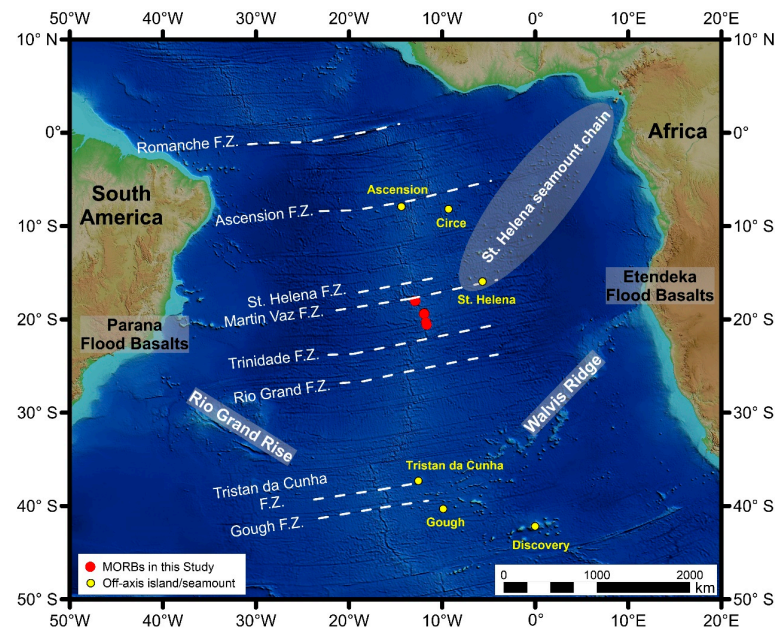


Figure 1. Geological background and the locations of study samples. Red circles represent new MORBs samples in this study and gray circles represent MORBs samples in previous studies. Off-axis islands and seamounts are shown by yellow circles. The cited island/seamount basalts data are downloaded from PetDB (<http://www.earthchem.org/petdb>; accessed on 31 May 2021).

3. Analytical Methods

3.1. Preparation

Prior to the geochemical analysis, samples were crushed into small chips less than 2 mm in size, where altered samples were removed under a binocular microscope. Then, the remaining rock fragments were placed in ultrapure water for ultrasonic cleaning with the water being changed every 15 min until it was clear after cleaning. The dried samples were placed in absolute ethanol for ultrasonic cleaning to remove the organic matter on the surface. After a second round of drying, the clean samples were handpicked again under a binocular microscope to avoid alteration. Finally, the clean rock fragments were ground to 200 mesh with an agate mortar for subsequent geochemical analysis.

3.2. Whole-Rock Major Element and Trace Element Analyses

Major element data for whole-rock samples were obtained by X-ray fluorescence (XRF) spectrometry on fused glass discs using a PANalytical AXIOS Minerals instrument at the Rock-Mineral Preparation and Analysis Lab, the Institute of Geology and Geophysics (IGG; Beijing, China), Chinese Academy of Sciences (CAS), following the procedures described similarly in [34]. Loss on ignition (LOI) was measured as the weight loss of the samples, which was obtained independently by igniting 0.5 g of dry sample aliquot in a porcelain crucible for 1.5 h at 1000 °C in a muffle furnace. Analysis results for the reference standard (GSR-3) for major elements are consistent with the recommended values within the analytical error, and detailed data are presented in Table S1.

Whole-rock trace element contents were analyzed using a PlasmaQuant-MS Elite ICP-MS instrument at the State Key Laboratory of Ore Deposit Geochemistry (SKLOGD), Institute of Geochemistry, Chinese Academy of Sciences (IGCAS), China. The powdered samples (50 mg) were dissolved with a 1 mL HF + 1 mL HNO₃ mixture in high-pressure Teflon bombs at ~185 °C for 35 h. Rh was used as an internal standard to monitor signal drift during counting. The analytical precision was generally better than 10%. Analysis results for three international reference standards (OU-6, AGV-2, and GBPG-1) for trace elements are consistent with the recommended values within the analytical error, and detailed data are presented in Table S1.

3.3. Nd-Hf Isotope Analyses

Nd isotope analysis was performed at the University of Science and Technology of China (USTC), Hefei, China, following the procedures described similarly in [35,36]. Whole-rock powders of approximately 100 mg were weighed and placed in 15 mL of Teflon stuffy tanks and dissolved in a mixture of 2–3 mL of purified HF solution and 8–10 drops of purified HClO₄ solution. Decomposition of refractory phases was ensured by heating the samples in a Teflon tank at 120 °C for approximately 7 days. After the samples were completely dissolved, the sample solutions were dried on a hot plate at 120 °C, and then heated to 150 °C to completely remove the HF and HClO₄. Next, 3 mL of purified 6 N HCl solution was added to the sample tanks two times to clear the inside of the tanks and then dried again. The sample residues were redissolved with 1 mL of purified 3 N HCl solution to prepare for chemical separation and purification. Light rare earth elements were isolated on quartz columns by conventional ion exchange chromatography with a 5-mL resin bed of Bio-Rad AG50W-X12, 200–400 mesh. Nd was separated from other rare earth elements on quartz columns using 1.7 mL of Teflon powder coated with HDEHP and di(2-ethylhexyl) orthophosphoric acid, as the cation exchange medium. All isotopic measurements were performed on a Finnigan MAT 262 mass spectrometer. Nd was loaded as phosphate on preconditioned Re filaments, and measurements were performed in a Re double filament configuration. The ¹⁴³Nd/¹⁴⁴Nd ratios were normalized to ¹⁴⁶Nd/¹⁴⁴Nd = 0.7219.

The measurement accuracies of the ¹⁴³Nd/¹⁴⁴Nd ratios for the samples were better than 0.003%. Procedural blanks were <100 pg for Nd. The precision for all the measured isotopic ratios is given in 2σ uncertainty. Details of the analytical uncertainties are presented in Table S2. During the period of data collection, repeated measurements on the Jndi standard solutions gave average ¹⁴³Nd/¹⁴⁴Nd ratios of 0.512115 ± 0.000006 (2σ, n = 7). The results of Nd isotopic analyses on the standard materials BCR-2 and AGV-2 (basalt powder) gave average ¹⁴³Nd/¹⁴⁴Nd ratios of 0.512635 ± 0.000009 (2σ, n = 2) and 0.512789 ± 0.000009 (2σ, n = 2).

Whole-rock Hf isotopic analysis was performed at Guizhou Tongwei Analytical Technology Co., Ltd., China. About 50–100 mg of rock powder samples were dissolved with a mixture of concentrate nitric acid and hydrofluoric acid in Teflon bombs at 185 °C in the oven for 3 days, and dried on a hot plate at 80 °C. Hf was initially washed from the column using a mixture of 0.2 N HBr + 0.5 N HNO₃ (collected) and was separated using a Bio-Rad AG50W-X8 cation exchange column (Bio-Rad Laboratories, Hercules, CA, USA). Hf was first washed using 1.5 N HCl (collected), then was collected on a column using HDEHP(di(2-ethylhexyl)-coated Teflon powder. The previously collected HFSE Hf was heated until dry and then redissolved in 3.0 N HCl. Finally, Hf was extracted from the column using 2.0 N HF and collected in a 10 mL PFA (preconditioned perfluoroalkoxy) beaker. The Hf-bearing elution was gently evaporated until dry and subsequently redissolved in 1.0 mL of 2 wt% HNO₃. These diluted solutions were introduced into a Nu Plasma HR MC-ICP-MS with a DSN-100 dissolution nebulizing system to determine the whole-rock Hf isotopic composition. Instrument bias and mass fractionation were corrected by normalization raw ratios to ¹⁷⁹Hf/¹⁷⁷Hf = 0.7325. Seven measurements of W-2a and BHVO-2 yielded average ratios of ¹⁷⁶Hf/¹⁷⁷Hf = 0.282741 ± 7 (2σ, n = 7) and 0.283103 ± 6 (2σ, n = 7).

Analysis results for these international reference standards for Nd-Hf isotopes are consistent with the recommended values, which can be found in GeoReM (georem.mpch-mainz.gwdg.de), within the analytical error.

4. Results

4.1. Major and Trace Elements

All 16 samples were analyzed for whole-rock major and trace elements and yielded low LOI values (<0.5 wt%; Table S1), suggesting that the samples were fresh. The major oxide contents described below were recalculated on an LOI-free basis. The content of MgO is 7.37–9.56 wt%, and the average MgO content is 8.4 wt%, suggesting that the samples

were less affected by low-pressure crystallization. All samples are plotted in the basalt area in a total alkali vs. silica (TAS) plot, and are classified as low-K subalkaline basalts (Figure 2).

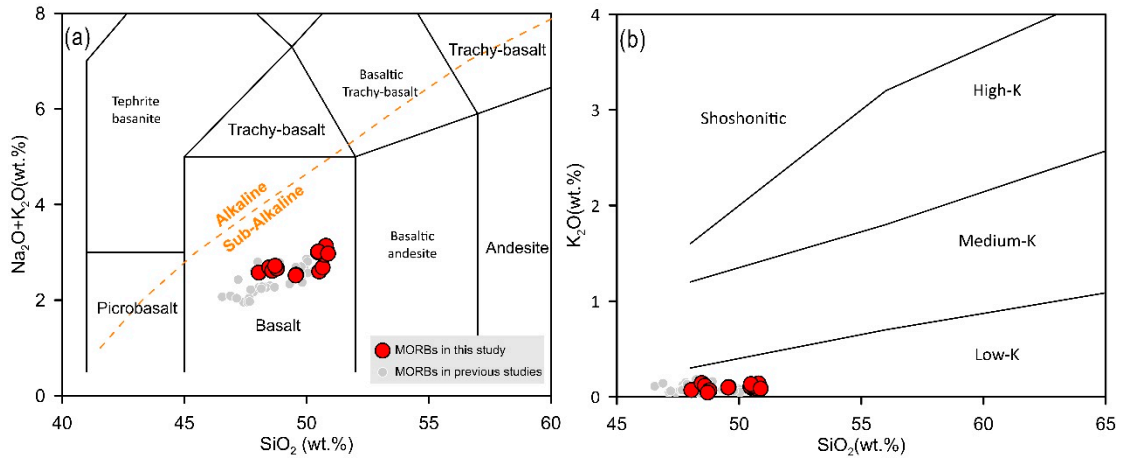


Figure 2. (a) Total alkali vs. SiO₂ diagram. The alkaline-subalkaline discrimination line is from [37]. (b) K₂O vs. SiO₂ diagram. The discrimination lines are from [38]. The red and gray circles represent the SMAR basalts in this study and in previous studies [26,32,39], respectively. Primitive mantle and N-MORB data are from [40].

The (La/Sm)_N (“N” denotes normalization to chondrite) ratio of the samples ranges from 0.49 to 0.79, and the Zr/Nb ratio ranges from 17.1 to 79.1, which indicate that the samples belong to the typical N-MORB. Figure 3a shows the primitive mantle-normalized trace element patterns of the study samples. In addition to the highly incompatible elements expected to be heavily depleted overall, the most remarkable feature is that all samples have clear positive anomalies of U and Pb (U/U* = 1.05–3.52, Pb/Pb* = 1.01–2.62; U* = (Th_N + Nb_N)/2, Pb* = (Ce_N + Pr_N)/2; “N” denotes normalization to the primitive mantle), negative anomalies of Nb, and Rb enrichment in some samples. The chondrite-normalized REE patterns diagram (Figure 3b) shows that most samples are depleted in LREE, and some samples have a relatively flat REE pattern or even a slight depletion of HREE. Meanwhile, most samples have negative Eu anomalies, with the lowest Eu/Eu* (Eu* = (Sm_N + Gd_N)/2; “N” denotes normalization to the primitive mantle) being 0.86.

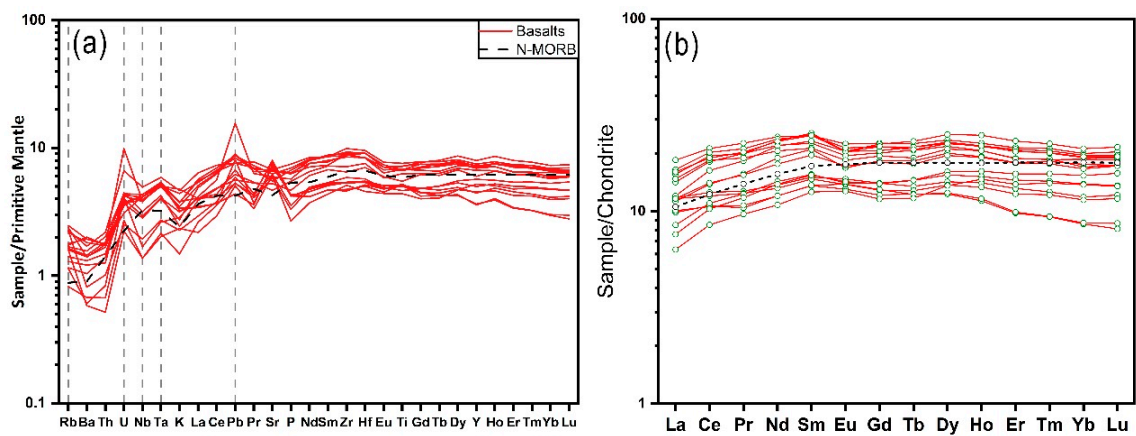


Figure 3. (a) Primitive mantle-normalized trace element patterns for the analyzed samples. (b) Chondrite-normalized trace element patterns for the analyzed samples. Primitive mantle, chondrite, and N-MORB data are from [40].

4.2. Nd-Hf Isotopic Compositions

All sixteen samples were analyzed for whole-rock Nd isotopic composition and eight samples were analyzed for whole-rock Hf isotopic composition. The isotope data are shown in Table S2. $^{143}\text{Nd}/^{144}\text{Nd}$ ratio ranges from 0.513030 to 0.513176, and $^{176}\text{Hf}/^{177}\text{Hf}$ ratio ranges from 0.282960 to 0.283188, which are in the range of previous studies [26,33], and confirm their geochemically depleted character. ϵNd - ϵHf plot (Figure 4) shows that all samples are plotted below the mantle array and were positively correlated.

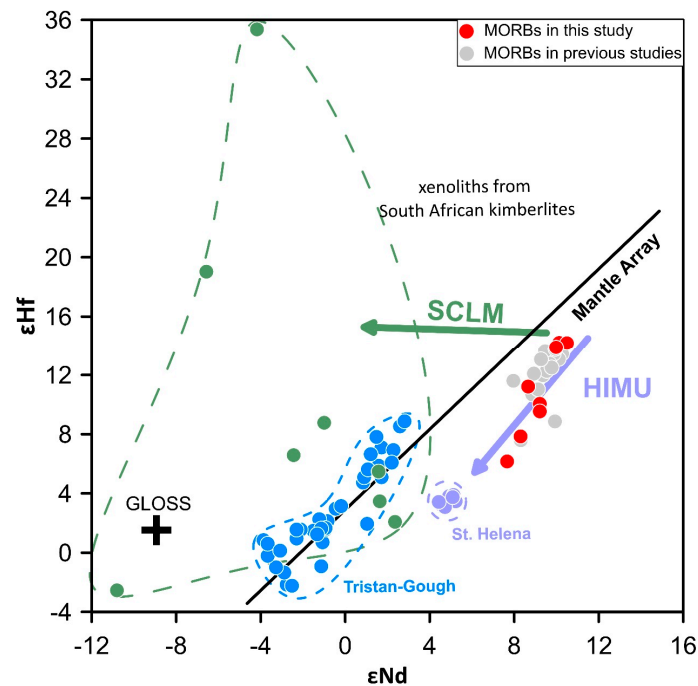


Figure 4. Plots of ϵNd vs. ϵHf . Red dots represent new MORBs in this study and gray dots represent SMAR 18–21°S MORBs in [26,32,39]. Black cross represents global subducting sediment (GLOSS), the composition of which is from [41,42]. The purple area represents the basalts of St. Helena seamount chain, and represents HIMU end-member. The blue area represents the basalts of Walvis ridge, and represents EM1 component. The green area represents the low-temperature garnet-peridotite xenoliths from Cretaceous South African kimberlites, and represents SCLM. The basalts from the St. Helena and the Tristan-Gough plumes are from PetDB (<http://www.earthchem.org/petdb>), the xenoliths from Cretaceous South African kimberlites are from [43]. Nd-Hf mantle array is from [44].

5. Discussion

5.1. Abnormal Trace Element Ratios

Ce/Pb and Nb/U ratios are relatively uniform in MORBs worldwide [13,24] at 25 ± 5 and 47 ± 10 (black dashed lines in Figure 5; [45]), respectively. However, Ce/Pb and Nb/U ratios in our samples vary widely (Figure 5), with an average value of 18 and 29, respectively. Figure 5 shows that regardless of the degree of depletion, Ce/Pb and Nb/U ratios of our samples are lower than the corresponding values (25 for Ce/Pb, 47 for Nb/U), with the lowest values of 9 and 13, respectively, which corresponds to the clear enrichment of U and Pb in the samples. In general, Ce/Pb ratio is positively correlated with Nb/U ratio (correlation coefficient is 0.63).

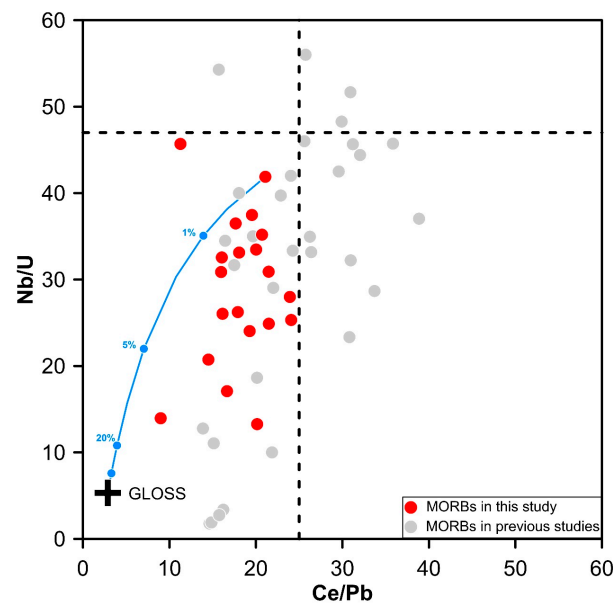


Figure 5. Plots of Ce/Pb vs. Nb/U. Red dots represent new MORBs in this study and gray dots represent SMAR 18–21°S MORBs in [26,32,39]. Black cross represents global subducting sediment (GLOSS), the composition of which is from [41]. Two dashed lines intersect at Nb/U = 47 and Ce/Pb = 25, which are from [13]. The blue line is the mixing line between GLOSS and SMAR-61. The details of end-members and mixing results are shown in Table S3.

The ratio of fluid-mobile element to fluid-immobile element, such as Ba/Nb (3.4–4.8), Ba/Th (59.7–94.6), Rb/La (0.22–0.71), Rb/Nb (0.35–1.04) ratios, was higher than the typical N-MORB (2.7 for Ba/Nb, 52.5 for Ba/Th, 0.22 for Rb/La, 0.24 for Rb/Nb; [40]). The plot of Rb/Nb vs. Ba/Nb (Figure 6a) shows that the Rb/Nb ratio is positively correlated with the Ba/Nb ratio (correlation coefficient is 0.62), except for the Rb-enriched MORBs. In the plot of Rb/La vs. Ba/Th (Figure 6b), Rb/La ratio of our samples is significantly positively correlated with Ba/Th ratio (correlation coefficient is 0.80).

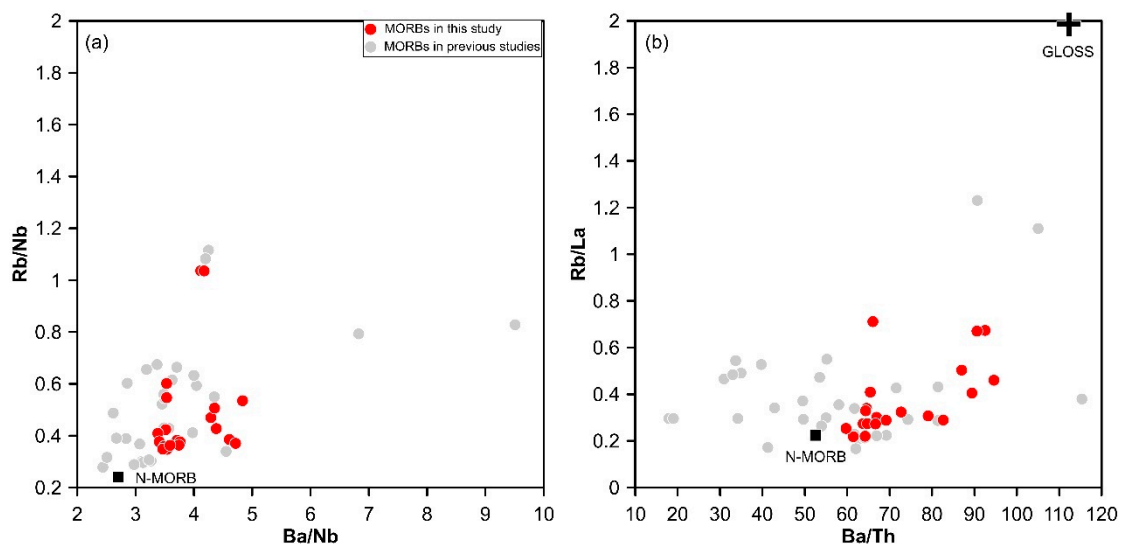


Figure 6. Plots of (a) Ba/Nb vs. Rb/Nb. (b) Ba/Th-Rb/La. Red dots represent new MORBs in this study and gray dots represent SMAR 18–21°S MORBs in [26,32,39]. Black square represents the typical N-MORB, the composition of which is from [40]. Black cross represents global subducting sediment (GLOSS), the composition of which is from [41].

Combined with the concentration of fluid-mobile elements, such as U and Pb, in the samples, subduction-related fluid process is a potential explanation for the abnormal trace elements ratios. In addition, continental crust material [46], recycled sediments [41], subduction modified mantle [47–50] have high Ba/Nb, Ba/Th, Rb/La, and Rb/Nb ratios, and higher U and Pb contents. Their injection into the mantle can also be the cause of this compositional anomaly. In addition to the above reasons, Le Roux et al. [51] proposed that the direct supply of mantle plume material was one of the reasons for the changes in some trace element ratios in MORBs.

5.2. The origin of Trace Element Anomalies

5.2.1. Continental Crust and SCLM

The continental crust materials have similar trace element characteristics as the samples in this study, such as low Ce/Pb and Nb/U ratios, high U and Pb contents and Ba/Nb, Ba/Th, Rb/La, and Rb/Nb ratios [46]. Furthermore, delaminated lower continental crust (LCC) has been found in the mantle beneath East Pacific Rise (EPR), Southeast Indian ridge (SEIR), and mid-Atlantic ridge (MAR) [10,12,15,16,52]. Therefore, the continental crust material is a possible origin of the trace element anomalies. In addition, the Atlantic Ocean was formed by the breakup of the west Gondwana [25]; therefore, the addition of SCLM should also be considered.

The addition of continental crust can significantly reduce the Nb/U ratio in the upper mantle, thus obtaining the trace element compositions consistent with the observed phenomenon. However, the ϵNd value of LCC is significantly lower than the MORB source [17]. Therefore, the addition of continental crust also changes the Nd isotopic composition of the MORB source, and thus MORB presents a mixed curve in the Ce/Pb- ϵNd plot. Figure 7 shows that the Nb/U ratio of MORBs in this study changes dramatically (from 45.7 to 13.3) within a limited range of ϵNd values. This indicates that there is no identifiable continental crust material in the upper mantle beneath SMAR 18–21°S.

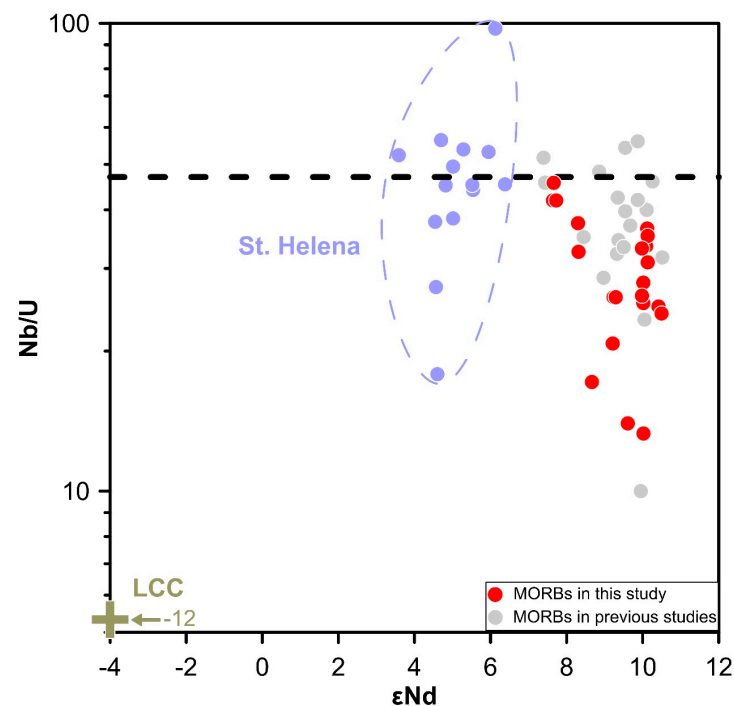


Figure 7. Plots of ϵNd vs. Nb/U. Red dots represent new MORBs in this study and gray dots represent SMAR 18–21°S MORBs in [26,32]. Black square represents the typical N-MORB, the composition of which is from [40]. Olive cross represents mean isotopic composition of mafic granulite which is from [17] and references therein.

Hanan et al. [16] proposed that the occurrence of LCC material in a MORB source would decouple the Nd-Hf isotopes of MORBs, and make MORB plots point to the position above the Nd-Hf mantle array in the $\epsilon\text{Nd}-\epsilon\text{Hf}$ plot. As shown in Figure 4, the samples have good correlation and all fall under the Nd-Hf mantle array. This is consistent with our conclusion that there is no identifiable continental crust material in the upper mantle of the study area.

For the reason of up to 3 Ga of radiogenic ingrowth following multiple episodes of mantle metasomatism, underplating, and melt extraction events, subcontinental lithosphere is isotopically heterogeneous [51]. However, SCLM beneath south Africa shows a strong subduction zone geochemical signature [53–55], with a relative depletion in Nb. Therefore, SCLM seems to be another possible origin of the trace element anomalies. Garnet and clinopyroxene are the main major host minerals for Nd and Hf in the mantle with concentrations mostly in the range of 0.01–15 (up to ~50) ppm Nd and 0.001–2 (up to ~8) ppm Hf in clinopyroxene, and 0.01–5 (up to ~20) ppm Nd and 0.02–1.5 (up to ~2.5) ppm Hf in garnet. Hf isotopic compositions of garnet and clinopyroxene are generally more radiogenic for their enrichment in Lu [43]. Therefore, the injection of SCLM will lead to a higher ϵHf value at a given ϵNd value. Whole-rock Nd-Hf isotope data for low-temperature garnet-peridotite xenoliths from Cretaceous South African kimberlites were plotted in Figure 4. The result shows that SCLM was distant from the trend formed by the SMAR 18–21°S MORB samples; therefore, there was no clear influence of subcontinental lithospheric mantle in the mantle beneath SMAR 18–21°S. In addition, Hanan et al. [16] ruled out the influence of SCLM since the amount of SCLM required to cause a clear abnormal ratio of trace elements was significantly large.

5.2.2. Direct Supply of Mantle Plume Material

Ridge-plume interaction is an important cause of mantle heterogeneity. If the mantle plume exists near the mid-ocean ridge, the mantle plume material will affect the mantle beneath the mid-ocean ridge, increasing the degree of isotopic heterogeneity in the MORBs source that was relatively uniform [11,56,57]. The study area is located in the southwest extension direction of the St. Helena seamount chain, only about 750 km away from the seamount chain. Previous studies [26,28–30,32,33] proved that the mantle source was affected by the St. Helena plume through Sr-Nd-Pb isotope data and geophysical evidence. The purple area in Figure 4 represents the isotopic composition region of the basalt produced by the St. Helena plume. Figure 4 shows that the Nd and Hf isotopes of the MORB samples are well correlated, and point to the St. Helena plume area, which is consistent with previous conclusions.

Le Roux et al. [51] proposed that some anomalies of trace elements in MORBs were caused by the direct supply of adjacent plume materials. If the anomalies of trace elements in this study are caused by the direct supply of plume materials, the basalts produced by the mantle plume should generally have low Ce/Pb and Nb/U ratios. However, Figure 7 shows that only few St. Helena basalts have a low Nb/U ratio, while most have a constant Nb/U ratio typical of oceanic basalts, with an average Nb/U ratio of 44, which is consistent with previous studies [13,23,24]. The injection of plume materials cannot reduce the Nb/U ratio of source mantle. Moreover, suppose that the direct supply of plume materials really is the origin of the trace element anomalies, the abnormal trace element ratios should be related to the isotopes. Namely, the more radioactive the isotopic composition of MORB is, the more clear the abnormal ratio of the trace elements will be. However, the correlation between the ratio of trace elements and isotopic composition is not clear (Figure 8). Therefore, the direct supply of St. Helena material does not result in the abnormal trace element ratios.

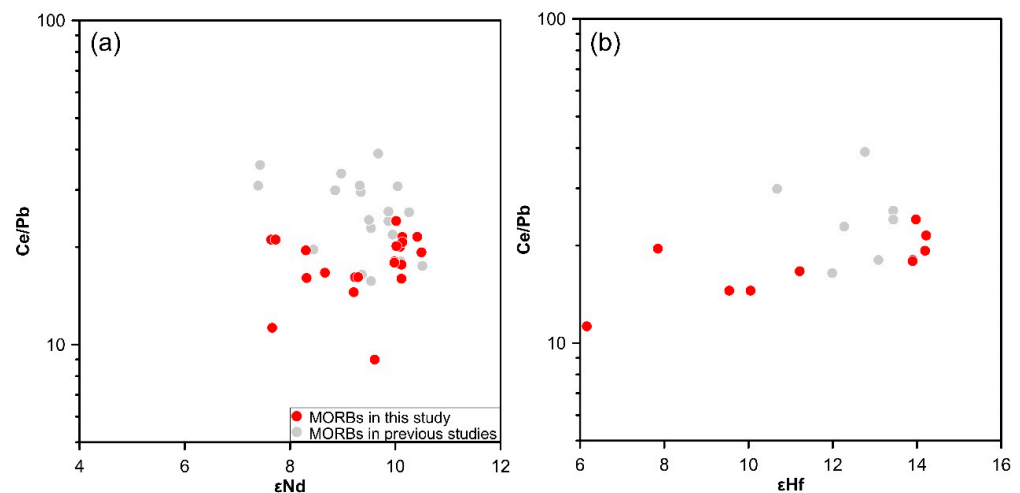


Figure 8. Plots of (a) ϵNd (b) ϵHf vs. Nb/U. Red dots represent new MORBs in this study and gray dots represent SMAR 18–21°S MORBs in [26,32].

5.2.3. Recycled Sediments

Sediments can be subducted into the mantle and thus affect the geochemical characteristics of the mantle [58,59]. The composition of subducted sediments is highly variable [41,60], but in general, recycled sediments have identifiable trace element and isotope characteristics. Therefore, recycled sediments are commonly used to explain the isotope and trace element system in MORB [42,51,52,61,62].

The plot of the GLOSS in Figures 4, 5 and 6b is located in the extension direction of the MORB sample array, and seems to indicate that it contributes to the source. However, after quantitative modeling (Figure 5), it was found that at least 10–20% of the sediment in the source was required to produce the observed trace element ratio anomalies. Even in BABB, such as the Manus Basin, the proportion of sediment is only <5% [63]. Clearly, the presence of this large proportion of sediments in the mantle beneath the mid-ocean ridge, which is distant from the subduction zone, is unreasonable. Moreover, due to the high ratio of $^{87}\text{Sr}/^{86}\text{Sr}$ in the sediments [41], this proportion of the sediments would cause the Sr isotopic composition of the samples to deviate significantly from the MORB range. Previous data [26,32,33] showed that the Sr isotopic composition (0.702398–0.702996, except for SA4A in [33]) in SMAR 18–21°S MORBs was not significantly higher than the normal MORB range. Therefore, we ruled out the sediment as an option. In addition, the Sr/Nd ratio of the sample (10.6–27.7, average 17.6) did not support the presence of recycled sediment (~12, [41]) in the source.

5.2.4. Subduction

The subduction signals of MORB or OIB are often interpreted as the result of the processes through which subduction directly affects the source mantle [21] or the existence of subduction modified mantle [17,61,64] in the source, and the Ba/Nb ratio is one of the most common indicators of subduction signals [65]. In our study, although the Ba/Nb ratio of our samples did not reach the standard (Ba/Nb > 6) of the BABB filter proposed by Yang et al. [21], it is still significantly higher than the typical N-MORB (Ba/Nb ~2.7; [40]). Considering that the study area is affected by the St. Helena plume, the addition of plume material will weaken the subduction signal in the study area. Therefore, we cannot rule out the possibility that the mantle in the study area is affected by subduction only by the fact that the Ba/Nb ratio is not sufficiently enough. In addition, Nb negative anomalies are important indicators of subduction, which are commonly seen in rocks produced in back-arc basins, island arcs, and other subduction-associated tectonic environments [47,63].

Furthermore, Ba/Th and Th/Nb ratios can be used to indicate the influence of subduction fluid and melt, respectively [48,51,65]. Ba/Nb vs. Ba/Th, Ba/Nb vs. Th/Nb plots

(Figure 9) show that the variation of Ba/Nb ratio in the samples was mainly controlled by the variation of Ba/Th ratio. Moreover, Ba/Th vs. Th/Nb plot (Figure 10) shows that if the study area is indeed affected by subduction, it should be mainly affected by the subduction fluid. Most of the subduction fluids are released shallowly in the subduction zone [66]; therefore, we can rule out the direct effects of the subduction zone. The spatially and temporally closest subduction zone which subducts/subducted toward the present SMAR 18–21°S is the eastern Pacific subduction zone, but the subduction zone and SMAR 18–21°S were separated by the South American continent, even before the south Atlantic opened. As the Atlantic opens, the distance becomes increasingly larger. For shallow subduction fluids to be directly affected in this distance, it would require an unreasonably small subducted angle and an extremely long subducted distance. Therefore, the hypothesis that the subduction of the eastern Pacific directly affects the source mantle is ruled out. The ancient subduction zone associated with the Rheic Ocean was located on the northern side of Africa and South America [67,68]. Similar to the eastern Pacific subduction zone, subduction fluids are difficult to be affected in the study area due to the distance. Therefore, only the process of subduction modified mantle transmitted to the study area through the mantle convection can make sense.

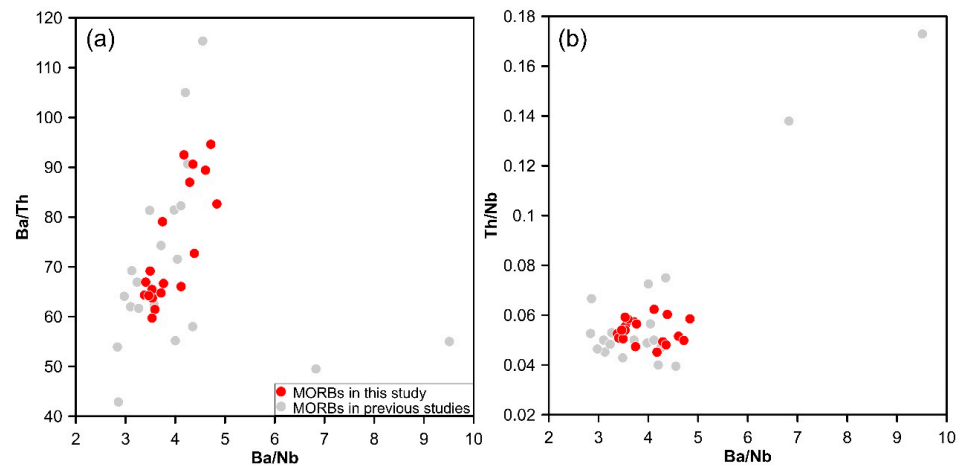


Figure 9. Plots of Ba/Nb vs. (a) Ba/Th (b) Th/Nb. Red dots represent new MORBs in this study and gray dots represent SMAR 18–21°S MORBs in [26,32].

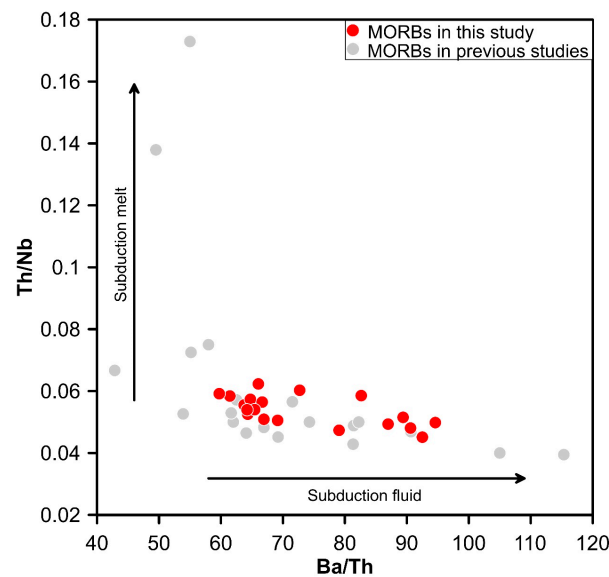


Figure 10. Plots of Ba/Th vs. Th/Nb. Red dots represent new MORBs in this study and gray dots represent SMAR 18–21°S MORBs in [26,32].

6. Conclusions

In this study, 16 basalt samples from 14 sites on the axis of SMAR 18–21°S were collected and analyzed for the composition of major element, trace element, and Nd-Hf isotope. The results are shown as follows:

1. These samples belong to the low-K subalkaline basalt, which is classified into N-MORB according to the $(La/Sm)_N$ ratio, and Nd-Hf isotope composition shows the characteristics of depletion. However, compared with typical N-MORB samples, the fluid-mobile elements, such as U, Pb, and Rb are enriched. Meanwhile, Ce/Pb and Nb/U ratios are higher than the constant value, while Ba/Nb, Ba/Th, Rb/La, Rb/Nb, and other trace element ratios are significantly higher than the typical N-MORB. In addition, our samples all have negative anomalies of Nb.
2. Plot of $\epsilon Nd-\epsilon Hf$ shows that the mantle beneath SMAR 18–21°S is affected by the St. Helena plume. However, the anomalies of trace element in the samples are not caused by the direct supply of plume material. In addition, we exclude the possibility of continental crust material, subcontinental lithospheric mantle, and recycled sediments. Furthermore, we propose that the anomalies of trace element are related to subduction.

The influence of subduction on the samples is mainly caused by the subduction fluid. Based on the geographical location, it seems unreasonable that the subduction directly affects the mantle beneath SMAR 18–21°S. It is more likely that the mantle modified by the subduction fluid is transmitted to the mantle beneath SMAR 18–21°S through mantle convection.

Supplementary Materials: The following supporting information can be downloaded at: <https://www.mdpi.com/article/10.3390/jmse11020441/s1>, Table S1: Whole rock major and trace elements compositions; Table S12: Whole Rock Nd-Hf isotopic compositions; Table S3: The mixing calculations of ratios of trace element between GLOSS and SMAR-61.

Author Contributions: Conceptualization, T.J. and Z.Z.; methodology, T.J.; software, T.J.; validation, T.J.; formal analysis, T.J.; investigation, T.J. and Z.Z.; resources, Z.Z.; data curation, T.J.; writing—original draft preparation, T.J.; writing—review and editing, T.J. and Z.Z.; visualization, T.J.; supervision, Z.Z.; project administration, Z.Z.; funding acquisition, Z.Z. All authors have read and agreed to the published version of the manuscript.

Funding: This research received no external funding or This research was funded by the National Natural Science Foundation of China (Grant No. 91958213), Strategic Priority Research Program (B) of the Chinese Academy of Sciences (Grant No. XDB42020402), National Basic Research Program of China (Grant No. 2013CB429700), and the Taishan Scholars Program.

Informed Consent Statement: Not applicable.

Data Availability Statement: All the data are given in the Supporting Information.

Acknowledgments: We are grateful for the valuable comments and suggestions from the anonymous reviewers and editors. This work was supported by the National Natural Science Foundation of China (Grant No. 91958213), Strategic Priority Research Program (B) of the Chinese Academy of Sciences (Grant No. XDB42020402), National Basic Research Program of China (Grant No. 2013CB429700), and the Taishan Scholars Program.

Conflicts of Interest: The authors declare no conflict of interest.

References

1. Zindler, A.; Hart, S.R. Chemical Geodynamics. *Ann. Rev. Earth Planet. Sci.* **1986**, *14*, 493–571. [[CrossRef](#)]
2. Hart, S.R. Heterogeneous Mantle Domains: Signatures, Genesis and Mixing Chronologies. *Earth Planet. Sci. Lett.* **1988**, *90*, 273–296. [[CrossRef](#)]
3. Willbold, M.; Stracke, A. Trace Element Composition of Mantle End-members: Implications for Recycling of Oceanic and Upper and Lower Continental Crust. *Geochem. Geophys. Geosyst.* **2006**, *7*, 2005GC001005. [[CrossRef](#)]
4. White, W.M. Isotopes, DUPAL, LLSVPs, and Anekantavada. *Chem. Geol.* **2015**, *419*, 10–28. [[CrossRef](#)]
5. Workman, R.K.; Hart, S.R. Major and Trace Element Composition of the Depleted MORB Mantle (DMM). *Earth Planet. Sci. Lett.* **2005**, *231*, 53–72. [[CrossRef](#)]

6. Dupré, B.; Allègre, C.J. Pb–Sr Isotope Variation in Indian Ocean Basalts and Mixing Phenomena. *Nature* **1983**, *303*, 142–146. [[CrossRef](#)]
7. Hart, S.R. A Large-Scale Isotope Anomaly in the Southern Hemisphere Mantle. *Nature* **1984**, *309*, 753–757. [[CrossRef](#)]
8. Pearce, J.A.; Kempton, P.D.; Nowell, G.M.; Noble, S.R. Hf–Nd Element and Isotope Perspective on the Nature and Provenance of Mantle and Subduction Components in Western Pacific Arc–Basin Systems. *J. Petrol.* **1999**, *40*, 33. [[CrossRef](#)]
9. Niu, Y.; Bideau, D.; Hékinian, R.; Batiza, R. Mantle Compositional Control on the Extent of Mantle Melting, Crust Production, Gravity Anomaly, Ridge Morphology, and Ridge Segmentation: A Case Study at the Mid-Atlantic Ridge 33–35° N. *Earth Planet. Sci. Lett.* **2001**, *186*, 383–399. [[CrossRef](#)]
10. Meyzen, C.M.; Ludden, J.N.; Humler, E.; Luais, B.; Toplis, M.J.; Mével, C.; Storey, M. New Insights into the Origin and Distribution of the DUPAL Isotope Anomaly in the Indian Ocean Mantle from MORB of the Southwest Indian Ridge: INDIAN OCEAN DUPAL ISOTOPE ANOMALY. *Geochem. Geophys. Geosyst.* **2005**, *6*, Q11K11. [[CrossRef](#)]
11. Gale, A.; Laubier, M.; Escrig, S.; Langmuir, C.H. Constraints on Melting Processes and Plume–Ridge Interaction from Comprehensive Study of the FAMOUS and North Famous Segments, Mid-Atlantic Ridge. *Earth Planet. Sci. Lett.* **2013**, *365*, 209–220. [[CrossRef](#)]
12. Mougél, B.; Agranier, A.; Hemond, C.; Gente, P. A Highly Unradiogenic Lead Isotopic Signature Revealed by Volcanic Rocks from the East Pacific Rise. *Nat. Commun.* **2014**, *5*, 4474. [[CrossRef](#)] [[PubMed](#)]
13. Hofmann, A.W. Mantle Geochemistry: The Message from Oceanic Volcanism. *Nature* **1997**, *385*, 219–229. [[CrossRef](#)]
14. Kamenetsky, V.S.; Maas, R.; Sushchevskaya, N.M.; Norman, M.D.; Cartwright, I.; Peyve, A.A. Remnants of Gondwanan Continental Lithosphere in Oceanic Upper Mantle: Evidence from the South Atlantic Ridge. *Geology* **2001**, *29*, 243–246. [[CrossRef](#)]
15. Escrig, S.; Capmas, F.; Dupré, B.; Allègre, C.J. Osmium Isotopic Constraints on the Nature of the DUPAL Anomaly from Indian Mid-Ocean-Ridge Basalts. *Nature* **2004**, *431*, 59–63. [[CrossRef](#)]
16. Hanan, B.B.; Blichert-Toft, J.; Pyle, D.G.; Christie, D.M. Contrasting Origins of the Upper Mantle Revealed by Hafnium and Lead Isotopes from the Southeast Indian Ridge. *Nature* **2004**, *432*, 91–94. [[CrossRef](#)]
17. Janney, P.E.; Le Roex, A.P.; Carlson, R.W. Hafnium Isotope and Trace Element Constraints on the Nature of Mantle Heterogeneity beneath the Central Southwest Indian Ridge (13° E to 47° E). *J. Petrol.* **2005**, *46*, 2427–2464. [[CrossRef](#)]
18. Stracke, A.; Hofmann, A.W.; Hart, S.R. FOZO, HIMU, and the Rest of the Mantle Zoo: THE MANTLE ZOO. *Geochem. Geophys. Geosyst.* **2005**, *6*, Q05007. [[CrossRef](#)]
19. Stracke, A. Earth’s Heterogeneous Mantle: A Product of Convection-Driven Interaction between Crust and Mantle. *Chem. Geol.* **2012**, *330–331*, 274–299. [[CrossRef](#)]
20. Zhang, G.-L.; Luo, Q.; Zhao, J.; Jackson, M.G.; Guo, L.-S.; Zhong, L.-F. Geochemical Nature of Sub-Ridge Mantle and Opening Dynamics of the South China Sea. *Earth Planet. Sci. Lett.* **2018**, *489*, 145–155. [[CrossRef](#)]
21. Yang, A.Y.; Langmuir, C.H.; Cai, Y.; Michael, P.; Goldstein, S.L.; Chen, Z. A Subduction Influence on Ocean Ridge Basalts Outside the Pacific Subduction Shield. *Nat. Commun.* **2021**, *12*, 4757. [[CrossRef](#)] [[PubMed](#)]
22. Fang, W.; Dai, L.-Q.; Zheng, Y.-F.; Zhao, Z.-F. Molybdenum Isotopes in Mafic Igneous Rocks Record Slab–Mantle Interactions from Subarc to Postarc Depths. *Geology* **2022**, *51*, 3–7. [[CrossRef](#)]
23. Halliday, A.N.; Lee, D.-C.; Tommasini, S.; Davies, G.R.; Paslick, C.R.; Godfrey Fitton, J.; James, D.E. Incompatible Trace Elements in OIB and MORB and Source Enrichment in the Sub-Oceanic Mantle. *Earth Planet. Sci. Lett.* **1995**, *133*, 379–395. [[CrossRef](#)]
24. Hofmann, A.W.; Class, C.; Goldstein, S.L. Size and Composition of the MORB+OIB Mantle Reservoir. *Geochem. Geophys. Geosyst.* **2022**, *23*, e2022GC010339. [[CrossRef](#)]
25. Ito, G.; van Keken, P.E. Hot Spots and Melting Anomalies. In *Treatise on Geophysics*; Elsevier: Amsterdam, The Netherlands, 2007; pp. 371–435, ISBN 978-0-444-52748-6.
26. Zhang, H.; Yan, Q.; Li, C.; Shi, X.; Yang, Y.; Wang, G.; Hua, Q.; Zhu, Z.; Zhang, H.; Zhao, R. Tracing Material Contributions from Saint Helena Plume to the South Mid-Atlantic Ridge System. *Earth Planet. Sci. Lett.* **2021**, *572*, 117130. [[CrossRef](#)]
27. Wilson, M. Magmatism and Continental Rifting during the Opening of the South Atlantic Ocean: A Consequence of Lower Cretaceous Super-Plume Activity? *Geol. Soc. Lond. Spec. Publ.* **1992**, *68*, 241–255. [[CrossRef](#)]
28. Schilling, J.-G. Upper Mantle Heterogeneities and Dynamics. *Nature* **1985**, *314*, 62–67. [[CrossRef](#)]
29. Hanan, B.B.; Kingsley, R.H.; Schilling, J.-G. Pb Isotope Evidence in the South Atlantic for Migrating Ridge–Hotspot Interactions. *Nature* **1986**, *322*, 137–144. [[CrossRef](#)]
30. Fontignie, D.; Schilling, J.-G. Mantle Heterogeneities beneath the South Atlantic: A Nd–Sr–Pb Isotope Study along the Mid-Atlantic Ridge (3° S–46° S). *Earth Planet. Sci. Lett.* **1996**, *142*, 209–221. [[CrossRef](#)]
31. Storey, B.C. The Role of Mantle Plumes in Continental Breakup: Case Histories from Gondwanaland. *Nature* **1995**, *377*, 301–308. [[CrossRef](#)]
32. Zhang, H.; Shi, X.; Li, C.; Yan, Q.; Yang, Y.; Zhu, Z.; Zhang, H.; Wang, S.; Guan, Y.; Zhao, R. Petrology and Geochemistry of South Mid-Atlantic Ridge (19° S) Lava Flows: Implications for Magmatic Processes and Possible Plume–Ridge Interactions. *Geosci. Front.* **2020**, *11*, 1953–1973. [[CrossRef](#)]
33. Zhong, Y.; Zhang, X.; Sun, Z.; Liu, J.; Li, W.; Ma, Y.; Liu, W.; Xia, B.; Guan, Y. Sr–Nd–Pb–Hf Isotopic Constraints on the Mantle Heterogeneities beneath the South Mid-Atlantic Ridge at 18–21° S. *Minerals* **2020**, *10*, 1010. [[CrossRef](#)]
34. Xue, D.-S.; Su, B.-X.; Zhang, D.-P.; Liu, Y.-H.; Guo, J.-J.; Guo, Q.; Sun, J.-F.; Zhang, S.-Y. Quantitative Verification of 1:100 Diluted Fused Glass Beads for X-Ray Fluorescence Analysis of Geological Specimens. *J. Anal. At. Spectrom.* **2020**, *35*, 2826–2833. [[CrossRef](#)]

35. Chen, F.; Hegner, E.; Todt, W. Zircon Ages and Nd Isotopic and Chemical Compositions of Orthogneisses from the Black Forest, Germany: Evidence for a Cambrian Magmatic Arc. *Int. J. Earth Sci.* **2000**, *88*, 791–802. [[CrossRef](#)]
36. Chen, F.; Li, X.-H.; Wang, X.-L.; Li, Q.-L.; Siebel, W. Zircon Age and Nd–Hf Isotopic Composition of the Yunnan Tethyan Belt, Southwestern China. *Int. J. Earth Sci.* **2007**, *96*, 1179–1194. [[CrossRef](#)]
37. Irvine, T.N.; Baragar, W.R.A. A Guide to the Chemical Classification of the Common Volcanic Rocks. *Can. J. Earth Sci.* **1971**, *8*, 523–548. [[CrossRef](#)]
38. Rickwood, P.C. Boundary Lines within Petrologic Diagrams Which Use Oxides of Major and Minor Elements. *Lithos* **1989**, *22*, 247–263. [[CrossRef](#)]
39. Zhong, Y.; Liu, W.; Sun, Z.; Yakymchuk, C.; Ren, K.; Liu, J.; Li, W.; Ma, Y.; Xia, B. Geochemistry and Mineralogy of Basalts from the South Mid-Atlantic Ridge (18.0°–20.6° S): Evidence of a Heterogeneous Mantle Source. *Minerals* **2019**, *9*, 659. [[CrossRef](#)]
40. Sun, S.-S.; McDonough, W.F. Chemical and Isotopic Systematics of Oceanic Basalts: Implications for Mantle Composition and Processes. *Geol. Soc. Lond. Spec. Publ.* **1989**, *42*, 313–345. [[CrossRef](#)]
41. Plank, T.; Langmuir, C.H. Tracing Trace Elements from Sediment Input to Volcanic Output at Subduction Zones. *Nature* **1993**, *362*, 739–743. [[CrossRef](#)]
42. Chauvel, C.; Lewin, E.; Carpentier, M.; Arndt, N.T.; Marini, J.-C. Role of Recycled Oceanic Basalt and Sediment in Generating the Hf–Nd Mantle Array. *Nat. Geosci.* **2008**, *1*, 64–67. [[CrossRef](#)]
43. Bedini, R. Isotopic Constraints on the Cooling of the Continental Lithosphere. *Earth Planet. Sci. Lett.* **2004**, *223*, 99–111. [[CrossRef](#)]
44. Vervoort, J.D.; Blichert-Toft, J. Evolution of the Depleted Mantle: Hf Isotope Evidence from Juvenile Rocks through Time. *Geochim. Cosmochim. Acta* **1999**, *63*, 533–556. [[CrossRef](#)]
45. Hofmann, A.W.; Jochum, K.P.; Seufert, M.; White, W.M. Nb and Pb in Oceanic Basalts: New Constraints on Mantle Evolution. *Earth Planet. Sci. Lett.* **1986**, *79*, 33–45. [[CrossRef](#)]
46. Rudnick, R.L.; Gao, S. Composition of the Continental Crust. In *Treatise on Geochemistry*; Elsevier: Amsterdam, The Netherlands, 2014; pp. 1–51, ISBN 978-0-08-098300-4.
47. Park, S.-H.; Lee, S.-M.; Kamenov, G.D.; Kwon, S.-T.; Lee, K.-Y. Tracing the Origin of Subduction Components beneath the South East Rift in the Manus Basin, Papua New Guinea. *Chem. Geol.* **2010**, *269*, 339–349. [[CrossRef](#)]
48. Nielsen, S.G.; Shu, Y.; Auro, M.; Yogodzinski, G.; Shinjo, R.; Plank, T.; Kay, S.M.; Horner, T.J. Barium Isotope Systematics of Subduction Zones. *Geochim. Cosmochim. Acta* **2020**, *275*, 1–18. [[CrossRef](#)]
49. Richter, M.; Nebel, O.; Maas, R.; Mather, B.; Nebel-Jacobsen, Y.; Capitanio, F.A.; Dick, H.J.B.; Cawood, P.A. An Early Cretaceous Subduction-Modified Mantle underneath the Ultraslow Spreading Gakkel Ridge, Arctic Ocean. *Sci. Adv.* **2020**, *6*, eabb4340. [[CrossRef](#)]
50. Villalobos-Orchard, J.; Freymuth, H.; O'Driscoll, B.; Elliott, T.; Williams, H.; Casalini, M.; Willbold, M. Molybdenum Isotope Ratios in Izu Arc Basalts: The Control of Subduction Zone Fluids on Compositional Variations in Arc Volcanic Systems. *Geochim. Cosmochim. Acta* **2020**, *288*, 68–82. [[CrossRef](#)]
51. le Roux, P.J.; le Roex, A.P.; Schilling, J.-G.; Shimizu, N.; Perkins, W.W.; Pearce, N.J.G. Mantle Heterogeneity beneath the Southern Mid-Atlantic Ridge: Trace Element Evidence for Contamination of Ambient Asthenospheric Mantle. *Earth Planet. Sci. Lett.* **2002**, *203*, 479–498. [[CrossRef](#)]
52. Hanan, B.B.; Blichert-Toft, J.; Hemond, C.; Sayit, K.; Agranier, A.; Graham, D.W.; Albarède, F. Pb and Hf Isotope Variations along the Southeast Indian Ridge and the Dynamic Distribution of MORB Source Domains in the Upper Mantle. *Earth Planet. Sci. Lett.* **2013**, *375*, 196–208. [[CrossRef](#)]
53. Duncan, A.R. The Karoo Igneous Province—A Problem Area for Inferring Tectonic Setting from Basalt Geochemistry. *J. Volcanol. Geotherm. Res.* **1987**, *32*, 13–34. [[CrossRef](#)]
54. Turner, S.; Hawkesworth, C.; Gallagher, K.; Stewart, K.; Peate, D.; Mantovani, M. Mantle Plumes, Flood Basalts, and Thermal Models for Melt Generation beneath Continents: Assessment of a Conductive Heating Model and Application to the Paraná. *J. Geophys. Res.* **1996**, *101*, 11503–11518. [[CrossRef](#)]
55. Peate, D.W.; Hawkesworth, C.J.; Mantovani, M.M.S.; Rogers, N.W.; Turner, S.P. Petrogenesis and Stratigraphy of the High-Ti/Y Urubici Magma Type in the Parana Flood Basalt Province and Implications for the Nature of ‘Dupal’-Type Mantle in the South Atlantic Region. *J. Petrol.* **1999**, *40*, 451–473. [[CrossRef](#)]
56. Zhang, Y.-S.; Tanimoto, T. Ridges, Hotspots and Their Interaction as Observed in Seismic Velocity Maps. *Nature* **1992**, *355*, 45–49. [[CrossRef](#)]
57. Wei, X.; Zhang, G.-L.; Castillo, P.R.; Shi, X.-F.; Yan, Q.-S.; Guan, Y.-L. New Geochemical and Sr–Nd–Pb Isotope Evidence for FOZO and Azores Plume Components in the Sources of DSDP Holes 559 and 561 MORBs. *Chem. Geol.* **2020**, *557*, 119858. [[CrossRef](#)]
58. Tatsumi, Y. The Subduction Factory: How It Operates in the Evolving Earth. *Gsa Today* **2005**, *15*, 4. [[CrossRef](#)]
59. Sun, W.; Teng, F.-Z.; Niu, Y.-L.; Tatsumi, Y.; Yang, X.-Y.; Ling, M.-X. The Subduction Factory: Geochemical Perspectives. *Geochim. Cosmochim. Acta* **2014**, *143*, 1–7. [[CrossRef](#)]
60. Lin, P.-N. Trace Element and Isotopic Characteristics of Western Pacific Pelagic Sediments: Implications for the Petrogenesis of Mariana Arc Magmas. *Geochim. Cosmochim. Acta* **1992**, *56*, 1641–1654. [[CrossRef](#)]
61. Rehkamper, M.; Hofmann, A.W. Recycled Ocean Crust and Sediment in Indian Ocean MORB. *Earth Planet. Sci. Lett.* **1997**, *147*, 93–106. [[CrossRef](#)]

62. Ahmad, Q.; Wille, M.; Rosca, C.; Labidi, J.; Schmid, T.; Mezger, K.; König, S. Molybdenum Isotopes in Plume-Influenced MORBs Reveal Recycling of Ancient Anoxic Sediments. *Geochem. Persp. Lett.* **2022**, *23*, 43–48. [[CrossRef](#)]
63. Wang, X.; Huang, P.; Huang, H.; Hu, N. Geochemical and Isotopic Compositions of East Rift Lavas from the Manus Basin: Implications for the Origin of Subduction Components. *Geol. J.* **2020**, *55*, 7429–7442. [[CrossRef](#)]
64. Yu, H.-M.; Nan, X.-Y.; Wu, F.; Widom, E.; Li, W.-Y.; Kuentz, D.; Huang, F. Barium Isotope Evidence of a Fluid-Metasomatized Mantle Component in the Source of Azores OIB. *Chem. Geol.* **2022**, *610*, 121097. [[CrossRef](#)]
65. Leat, P.T.; Livermore, R.A.; Millar, I.L.; Pearce, J.A. Magma Supply in Back-Arc Spreading Centre Segment E2, East Scotia Ridge. *J. Petrol.* **2000**, *41*, 845–866. [[CrossRef](#)]
66. Grove, T.L.; Till, C.B.; Krawczynski, M.J. The Role of H₂O in Subduction Zone Magmatism. *Annu. Rev. Earth Planet. Sci.* **2012**, *40*, 413–439. [[CrossRef](#)]
67. Murphy, J.B.; Keppie, J.D.; Nance, R.D.; Dostal, J. Comparative Evolution of the Iapetus and Rheic Oceans: A North America Perspective. *Gondwana Res.* **2010**, *17*, 482–499. [[CrossRef](#)]
68. Nance, R.D.; Gutiérrez-Alonso, G.; Keppie, J.D.; Linnemann, U.; Murphy, J.B.; Quesada, C.; Strachan, R.A.; Woodcock, N.H. A Brief History of the Rheic Ocean. *Geosci. Front.* **2012**, *3*, 125–135. [[CrossRef](#)]

Disclaimer/Publisher’s Note: The statements, opinions and data contained in all publications are solely those of the individual author(s) and contributor(s) and not of MDPI and/or the editor(s). MDPI and/or the editor(s) disclaim responsibility for any injury to people or property resulting from any ideas, methods, instructions or products referred to in the content.